Microchemical Journal 222 (2026) 117286

Contents lists available at ScienceDirect

Microchemical Journal

journal homepage: www.elsevier.com/locate/microc

Combination of few-layer bismuthene and glutamate dehydrogenase for enhanced glutamate biosensing

Ana María Villa-Manso [a], Iñigo Torres [b], Félix Pariente [a,c], Encarnación Lorenzo [a,c,d], Félix Zamora [b], Eva Mateo-Martí [e], Cristina Gutiérrez-Sánchez [a,c,*], Mónica Revenga-Parra [a,c,*]

[a] Departamento de Química Analítica y Análisis Instrumental, Universidad Autónoma de Madrid, 28049 Madrid, Spain.
[b] Departamento de Química Inorgánica and Condensed Matter Physics Center (IFIMAC), Universidad Autónoma de Madrid, 28049 Madrid, Spain.
[c] Institute for Advanced Research in Chemical Sciences (IAdChem), Universidad Autónoma de Madrid, Madrid 28049, Spain.
[d] IMDEA-Nanociencia, Ciudad Universitaria de Cantoblanco, 28049 Madrid, Spain.
[e] Centro de Astrobiología (CSIC-INTA), Ctra. Ajalvir, Km. 4, 28850 Torrejón de Ardoz, Madrid, Spain.

ARTICLE INFO

Keywords:
Glutamate biosensor
Bismuthene
Screen-printed graphene electrode
Glutamate dehydrogenase

ABSTRACT

This work reports the development of an enzymatic electrochemical biosensor for glutamate detection based on few-layer bismuthene hexagons (FLB), a two-dimensional nanomaterial with outstanding electrocatalytic and biocompatible properties. FLB was synthesized by a wet chemistry method and integrated into screen-printed graphene electrodes (SPGrE) to provide a stable and biocompatible conductive surface for the immobilization of redox enzyme glutamate dehydrogenase (GLDH). The combination of FLB with GLDH enabled the efficient electrochemical detection of glutamate through the oxidation of enzymatically generated NADH. The resulting nanostructured biosensing platform exhibits a wide linear detection range (6.54–125 μM), a low detection limit (1.96 μM), and high selectivity toward common interfering compounds. Each step of the bioplatform fabrication was characterized using electrochemical, microscopic and spectroscopic techniques, confirming the successful immobilization of FLB and GLDH. The applicability of the biosensor was further validated by glutamate determination in human serum and food samples, demonstrating excellent analytical performance and storage stability over 20 days. These results highlight the potential of FLB as a key nanomaterial for the development of highly sensitive and selective enzymatic electrochemical biosensors.

1. Introduction

Glutamate is a non-essential amino acid that acts as an excitatory neurotransmitter of the central nervous system in vertebrates and is responsible for fundamental neurological processes such as memory formation and learning [1]. It also plays a crucial role in synaptic plasticity, as well as in the migration, differentiation, and death of cells in the forebrain [2]. However, elevated concentrations of this amino acid can induce neurotoxicity, leading to brain tissue damage and the development of neurological disorders such as schizophrenia [3], autism [4], multiple sclerosis [5], and neurodegenerative diseases including Alzheimer's and Parkinson's diseases [6,7]. In cellular metabolism, glutamate is a central molecule involved in protein synthesis and degradation. Moreover, it is essential for the proper functioning of various peripheral organs and tissues, contributing to cardiorespiratory, endocrine, and reproductive functions [8]. Therefore, the quantification of glutamate levels in brain tissue and biological fluids, such as cerebrospinal fluid or blood, is crucial, as it may support early disease diagnosis and provide valuable insights into disease progression.

Furthermore, glutamate is present in protein-rich foods such as meat, fish, cheese, milk, and vegetables. In addition, its sodium salt, monosodium glutamate (MSG), is widely used as food additive (E621) to enhance flavour and reduce salt content. It can also be used to mask ingredients of poor freshness [9]. Although generally recognized as safe, the use of monosodium glutamate in foods has long been controversial. Excessive consumption of this flavour enhancer may lead to a transient condition known as *Chinese Restaurant Syndrome*, characterized by symptoms such as severe headaches, nausea, palpitations, wheezing, and increased body temperature [10]. Controlled human studies have reported that these effects may occur in some individuals following

* Corresponding authors at: Departamento de Química Analítica y Análisis Instrumental, C/Francisco Tomás y Valiente, 7, Universidad Autónoma de Madrid, 28049 Madrid, Spain.
E-mail addresses: cristina.gutierrezs@uam.es (C. Gutiérrez-Sánchez), monica.revenga@uam.es (M. Revenga-Parra).

https://doi.org/10.1016/j.microc.2026.117286
Received 3 July 2025; Received in revised form 23 January 2026; Accepted 4 February 2026
Available online 9 February 2026

single oral doses of approximately 2.5–3 g of MSG, particularly when ingested without food, corresponding to intake levels of about 40–60 mg/kg body weight in adults [11]. On the other hand, high MSG intake has been associated with metabolic disorders, including diabetes and obesity. The use of glutamate as a food additive is regulated by the European Union, which has established a maximum permitted level of 10 g/kg. Moreover, the European Food Safety Authority has defined a group acceptable daily intake (ADI) of 30 mg/kg body weight per day, expressed as glutamic acid, and has noted that dietary exposure in some population groups may exceed the established ADI and approach levels at which adverse effects have been reported in humans [12]. Nevertheless, glutamate is often detected at high concentrations in food products that claim not to contain added glutamate [13,14]. For these reasons, the determination of glutamate or monosodium glutamate in food products is essential for assessing food quality and safety.

Several analytical methods have been developed for the detection of glutamate in various matrices, including high-performance liquid chromatography (HPLC) [15,16], capillary electrophoresis [17], UV–vis absorption spectrophotometry [18] and fluorescence spectrophotometry [19,20]. However, these techniques typically rely on expensive instrumentation and complex sample preparation procedures, resulting in long analysis times and significant reagent consumption, which limit their applicability for rapid and *in situ* analysis. In contrast, electrochemical methods, particularly enzymatic biosensors, represent a promising alternative, as their high selectivity and sensitivity enable more accurate measurements. Moreover, they require low-cost, simple instrumentation and are well suited for the development of small and portable analytical devices [21].

Nevertheless, appropriate enzyme immobilization strategies are required to develop an efficient enzymatic electrode. Therefore, it is advisable to optimize the coating of the active biocatalyst molecules on the electrode surface and to ensure high operational stability. It is also important to establish rapid electron transfer between the redox centers of the immobilized enzymes and the electrode. Electron transfer can be achieved using redox mediators, known as mediated electron transfer, or through direct electron transfer between the redox centers of the enzyme and the electrode. Many strategies have been proposed for the immobilization of different enzymes. One of them is the development of a matrix composed of hydrophobic ligands, referred to as superhydrophobic, which has been described to facilitate the interfacial activation of lipase [22]. Another one consists in the development of hydrophobic metal-organic structures and their modification with chains for the immobilization of lipase, which allowed it to adopt a stable open conformation on the surface of the support [23]. The design of a membrane enzyme immobilization procedure based on the insertion of its lipid tail into a phospholipid bilayer formed on the electrode surface is another approach [24,25]. Similarly, a nanostructured enzymatic electrode was prepared by gradual covalent attachment of gold nanoparticles and the enzyme onto porous graphite electrodes *via* electrochemical reduction strategy using diazonium salts. [26]. Lastly, the development of hollow nanospheres with a mesoporous biomimetic silica layer where the catalase enzyme exhibits an immobilized but not rigid state [27], or the synthesis of gold nanoparticles of controlled size using a tetradentate Schiff base ligand that, in addition to its reducing action, provided a suitable coating to the gold nanoparticles and the catalytic function to lactate oxidase, have been another strategies [28].

These biosensors are based on either glutamate oxidase (GLOx) or glutamate dehydrogenase (GLDH). GLOx efficiently catalyzes the oxidation of L-glutamate to α-ketoglutarate and hydrogen peroxide (H_2O_2). Several biosensors have been designed for glutamate detection based on this enzyme. For example, Hongtong Hu et al. constructed a mimetic multi-enzyme system combining GLOx and trimanganese tetroxide through biomineralization [29]. In another study, a nanobiocatalyst based on hybrid Fe_3O_4 nanoparticles incorporating GLOx was developed [30]. Additionally, an enzymatic hybrid nanoflowers, synthesized by a self-assembly biomineralization method, are another alternative used for the development of this type of biosensors based on the GLOx enzyme [31]. On the other hand, the enzyme GLDH catalyzes the reversible conversion of glutamate to α-ketoglutarate, using nicotinamide adenine dinucleotide (NAD^+) as a cofactor. Therefore, biosensors designed with GLDH are based on the detection of enzymatically generated NADH through its electrochemical oxidation. However, the kinetics of the direct oxidation of NADH at bare electrodes are slow, which means that a very positive potential must be applied to achieve oxidation. Another problem is the fouling of the electrode surface caused by the adsorption of oxidation products [32,33]. For these reasons, the development of electrochemical GLDH biosensors requires the use of electrodes modified with redox mediators capable of electrocatalysing NADH oxidation.

In this respect, in recent years, nanomaterials such as metal particles [34,35], carbon nanotubes [36,37], nanodiamonds [38] or carbon nanodots [39,40] have attracted great interest due to their ability to act as redox mediators, improving sensitivity and increasing the electroactive area of the working electrode. Recently, two-dimensional (2D) nanomaterials have attracted considerable attention from researchers due to their exceptional electronic, mechanical and optical properties, along with their high aspect ratio, quantum size effects, and planar surface configuration, which make them highly promising for various applications [41]. Accordingly, 2D nanomaterials such as graphene or transition metal dichalcogenides have been used in the fabrication of sensing devices [42,43]. The 2D layer structure and remarkable properties of monoelemental materials of group 15 of the periodic table, also known as pnictogens, make them excellent candidates for a wide range of applications, including (opto)electronics, energy, (bio)medicine, and sensing [44].

Pnictogens such as arsenene or antimonene, among others, have recently been used in the development of sensing platforms [45,46]. Similarly, bismuthene has shown superior properties compared to bismuth-based compounds, suggesting its potential use in photonic and electrical devices [47,48]. However, its application as a sensing platform is still underdeveloped, despite showing high electrochemical activity. In different studies, bismuthene has been employed to modify electrodes for the determination of heavy metal ions using anodic stripping voltammetry [49–52]. Moreover, bismuthene has been explored in the development of DNA and aptamer-based biosensors, taking advantage of its biocompatibility and favorable electrochemical properties for nucleic acid interactions. Notably, all these biosensors reported utilizing bismuthene have been designed for the detection of SARS-CoV-2, demonstrating its potential in bioanalytical applications related to infectious disease diagnostics [53–55]. However, its application in enzymatic biosensors or in sensors for the determination of organic compounds is still scarce. Mayorga-Martinez et al. were the first to develop an electrochemical biosensor for the determination of phenol using the enzyme tyrosinase and 2D pnictogens, including bismuthene [56]. The same research group, mixed shear exfoliated pnictogen nanosheets with silver shells and gold core nanorods as novel electrode materials for the development of a non-enzymatic electrochemical glucose sensor [57].

Our research group has previously demonstrated that few-layered bismuth hexagons (FLB), obtained by a two-step wet chemistry method, deposited onto screen-printed graphene electrodes (SPGrE) exhibit a high capacity for electron transfer. Based on these properties, a NADH sensor with good analytical performance was developed [58]. Taking advantage of these features and going a step further by focusing on improving selectivity, in this work we designed an enzymatic biosensor for the determination of glutamate. The analytical method relies on the use of a hybrid nanobioplatform prepared using FLB as a redox mediator, owing to its electrocatalytic activity toward NADH oxidation, and GLDH as biorecognition element. The synergy between nanomaterials and enzymes highlights the potential and versatility of FLB as a redox mediator for developing nanostructured biosensors based on dehydrogenase enzymes. This field has been relatively unexplored and holds significant promise for future research and applications. The

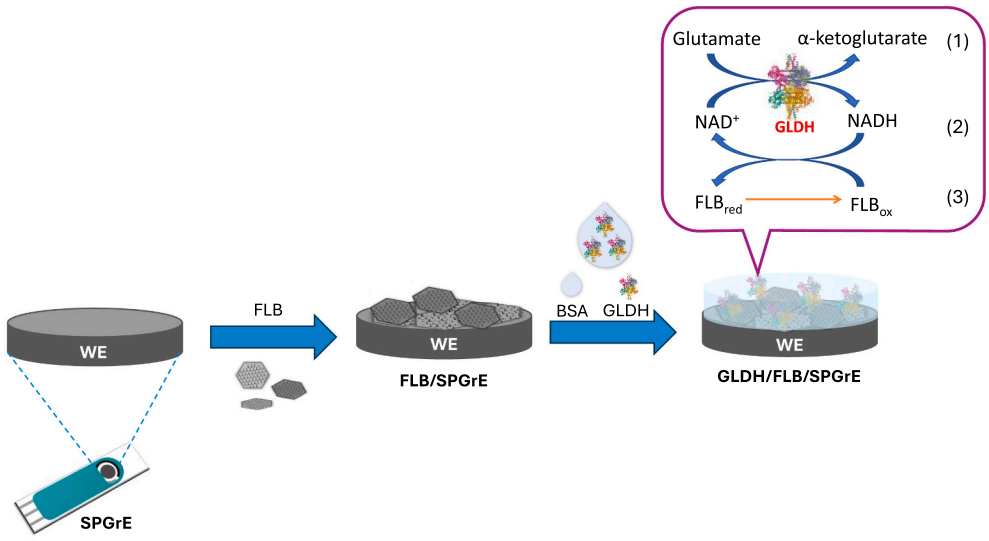

Scheme 1. Biosensor fabrication process.

resulting modified graphene electrode (GDH/FLB/SPGrE) was applied to the determination of glutamate in human serum and chicken bouillon cubes.

2. Experimental section

2.1. Chemicals and stock solution

Bismuth trichloride, octadecene (ODE) and dodecanethiol (DDT) were sourced from Alfa Aesar. HPLC-grade chloroform was supplied by Scharlab. Oleylamine (OA), L-glutamic acid monosodium salt monohydrate, potassium ferricyanide, potassium ferrocyanide, bovine serum albumin (BSA), glucose, L-ascorbic acid, taurine, L-lysine, uric acid, human serum, β-nicotinamide adenine dinucleotide reduced disodium salt hydrate (NADH), β-nicotinamide adenine dinucleotide sodium salt (oxidized form, NAD^+) and L-glutamic dehydrogenase (GLDH; EC 1.4.1.3 $\geq$ 35 U/mg protein; from bovine liver) were obtained from Merck. GLDH stock solutions (40 U/mL) were prepared in 0.1% (w/v) BSA in 0.1 M phosphate buffer (PB) pH 7.4 and aliquots were stored at −20 °C until use. Under these conditions the enzymatic activity remains stable for several weeks. The enzymatic assay kit for glutamate determination (K-GLUT 04/18) was purchased from Megazyme. Ultrapure water obtained from a Millipore Milli-Q system was used in all experiments.

2.2. Instrumentation

Atomic Force Microscopy (AFM) measurements were carried out using a Cervantes Full mode AFM from Nanotec Electronica SL in Si surfaces (with 300 nm of SiO_2 covering layer) sonicated in acetone for 15 min, subsequently in 2-propanol for another 15 min, and then dried under an argon flow. WSxM software (www.wsxmsolutions.com) was employed both for data acquisition and image processing [59,60]. Contact mode was used to acquire all the topographical images shown in this work to avoid possible artefacts in the flake thickness measurements [61]. PPP-NCHR cantilevers (nanosensors.com) with a nominal spring constant of 42 N m^{-1} and tip radius of less than 7 nm were employed. Low forces of the order of 1 nN were used for imaging to ensure that the flakes would not be deformed by the tip.

AFM studies of enzyme were performed with an Agilent 5500 microscope operating in tapping mode in air medium. The enzyme GLDH was deposited on FLB/SiO_2 substrates by dropcasting.

X-Ray Powder Diffraction patterns were measured on a Bruker D8 Advance with Cu Kα radiation with a rapid detector (lynxeye).

Raman spectroscopic characterization was carried out on a confocal Raman microscope with a spectral resolution of 0.02 cm^{-1}, coupled with an AFM instrument (Witec ALPHA 300RA), with laser excitation at 532 nm and a 100× objective lens (NA = 0.95). The incident laser power was 0.5 mW. The optical diffraction resolution was about 200 nm laterally and 500 nm vertically. The samples were mounted in a piezo-driven scan platform with 4 nm lateral and 0.5 nm vertical positioning accuracy, also equipped with an active vibration isolation system (0.7–1000 Hz). The spectra and images were processed and analyzed with the WiTec Project Plus 2.08 software. The Raman spectrums were carried out in Si substrates and screen-printed electrodes.

Transmission Electron Microscope (TEM) images on FLB in Si substrates were obtained in a JEOL JEM 2100 FX TEM system with an accelerating voltage of 200 kV in a Si substrate. The microscope has a multiscan charge-coupled device (CCD) camera ORIUS SC1000 and an OXFORD INCA X-Ray Energy Dispersive Spectroscopy (XEDS) microanalysis system. For the preparation of transmission electron microscopy samples, the product obtained by centrifugation was dispersed in $CHCl_3$ and deposited on lacey formvar/carbon copper grids (300 mesh).

The Scanning Electron Microscopy (SEM) images were acquired in an FE SEM Hitachi S-4700 operating at an accelerating voltage of 20 k.

X-Ray Photoelectron Spectroscopy (XPS) analysis of the three highly ordered pyrolytic graphite (HOPG) electrodes samples (FLB/HOPG, GLDH/HOPG y GLDH/FLB/HOPG) was carried out with a Phoibos 150 MCD spectrometer equipped with hemispherical electron analyzer, and using an Al Ka X-ray source (1486.7 eV) with an aperture of 7 mm × 20 mm. The base pressure in the ultra-high vacuum chamber was 2×10^{-9} mbar, and the experiments were carried out at room temperature. A 30 eV pass energy was applied for taking the over-view sample, whereas 20 eV pass energy was applied for the analysis of the following core level spectra: O(1s), C(1s), N(1s) and Bi(4f). XPS spectra regions were fitted and deconvoluted using the fit-xps software.

Electrochemical experiments were performed with an Autolab PGSTAT 30 potentiostat from Metrohm-Autolab, using integrated screen-printed graphene electrodes (SPGrEs; 4 mm diameter) from Metrohm-DropSens that include a silver pseudo-reference electrode and a graphene counter electrode. Electrochemical Impedance Spectroscopy (EIS) experiments were performed in 25 mM KCl containing an equimolar (10.0 mM) $K_3Fe(CN)_6/K_4Fe(CN)_6$ mixture. Impedance measurements were recorded in the 10^5–10^{-2} Hz frequency range, with a sinusoidal potential modulation of ±10 mV amplitude. Amperometric measurements of the biosensor (GLDH/FLB/SPGrE) were carried out in

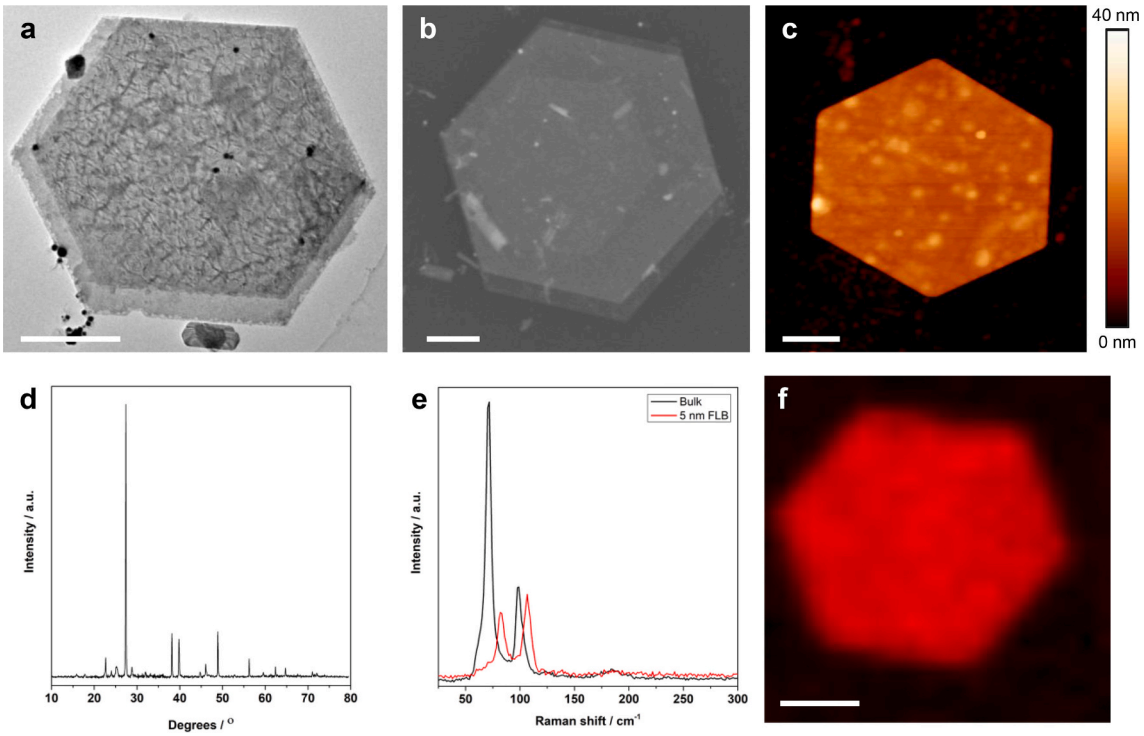

Fig. 1. (a) TEM image of a representative FLB hexagon. Scale bar of 1 μm. (b) SEM image of a representative FLB hexagon. Scale bar of 2 μm. (c) AFM image of a representative FLB hexagon with a thickness of 10 nm. Scale bar of 1 μm and colour scale bar of the height. (d) XRPD spectrum of the isolated FLB hexagons. (e) Raman spectra of bulk (black line) and an FLB hexagon of 5 nm thick (red line). (f) Raman mapping of an FLB hexagon. Scale bar of 1 μm. (For interpretation of the references to colour in this figure legend, the reader is referred to the web version of this article.)

0.1 M phosphate buffer (PB) (pH 7.4), containing 10.0 mM NAD^+ as a cofactor. The cofactor concentration used in this work was selected to ensure non-limiting cofactor conditions, as established in previous studies by the research group [40,62].

2.3. Procedures

2.3.1. Preparation of high-quality few-layers bismuthene hexagons (FLB)

In a typical synthesis, 315 mg (1 mmol) of $BiCl_3$ is added to a 100 mL three-necked flask. Under an argon atmosphere, 4 mL of DDT was introduced. The solution was subjected to vacuum until the salt is completely dissolved. Next, 6 mL of ODE is added under argon. The mixture is degassed under vacuum at 60 °C for 1 h. The resulting yellow solution was then heated under argon to 150 °C for 3 h. Subsequently, 1 mL of OA is added, and the reaction continues at 150 °C for 90 min. The mixture was then diluted with 40 mL of chloroform, centrifuged at 8000 rpm for 3 min, and washed three times with 50 mL of chloroform each time, centrifuging under the same conditions. Finally, the solid product was isolated under vacuum.

2.3.2. Modification of SPGrE with FLB hexagons (FLB/SPGrE)

Before the modification step, the FLB dispersion prepared in isopropanol at a concentration of 1.0 mg/mL was vortexed for a few minutes to ensure homogeneity before use. 10.0 μL of this dispersion was carefully deposited dropped onto SPGrE working electrode surface and was left to dry at room temperature. Afterwards, the modified electrodes (FLB/SPGrE) were stored at room temperature in the absence of light for further use.

2.3.3. Preparation of FLB/SPGrE modified with glutamate dehydrogenase (GLDH)

10.0 μL of the GLDH stock solution (11.4 μg of protein) were deposited on the FLB/SPGrE surface and placed for 1 h at 4 °C to assemble the enzyme on the electrode surface (GLDH/FLB/SPGrE). Prior to use, the platform was carefully rinsed in 0.1 M PB (pH 7.4) to eliminate molecules weakly adsorbed on the electrode surface (Scheme 1)

2.3.4. Determination of glutamate in samples

The developed amperometric biosensor was applied for the quantification of glutamate in human serum and commercial chicken bouillon cubes using the standard addition method. The serum samples were spiked and analyzed without any pretreatment beyond a simple dilution (100-fold) in 0.1 M PB (pH 7.4). For the food analysis, 1.000 g of finely ground bouillon cube was weighed and mixed with 70 mL of ultrapure water. Glutamate was extracted by heating the mixture at 70 °C for 10 min under constant stirring. Afterwards, the extract was adjusted to a final volume of 100.0 mL and filtered by gravity to remove any insoluble material. Before performing the chronoamperometric measurements, the sample was diluted 1:100 in 0.1 M PB (pH 7.4). The biosensor results were validated by comparison with a commercial enzymatic spectrophotometric assay kit, following the manufacturer's protocol.

3. Results and discussion

3.1. Characterization of FLB hexagons

The FLB hexagons were characterized using both morphological and spectroscopic techniques. TEM images reveal their hexagonal morphology and lateral dimensions exceeding one micron (Figs. 1a and S1). This morphology and size were further confirmed by SEM (Figs. 1b and S2). Additionally, AFM was employed to corroborate the morphology and assess the lateral sizes and thickness of the FLB hexagons (Fig. 1c). Statistical analysis of AFM images (Fig. S3) shows that most FLB hexagons exhibit thicknesses below 20 nm, lateral dimensions over 2 μm, and areas in the range of 4–10 μm^2 (Fig. S4).

Moreover, the structure of the FLB hexagons was assessed using XRPD spectroscopy, which confirmed the rhombohedral β-phase structure of bismuth (Fig. 1d). Raman spectroscopy was further employed to

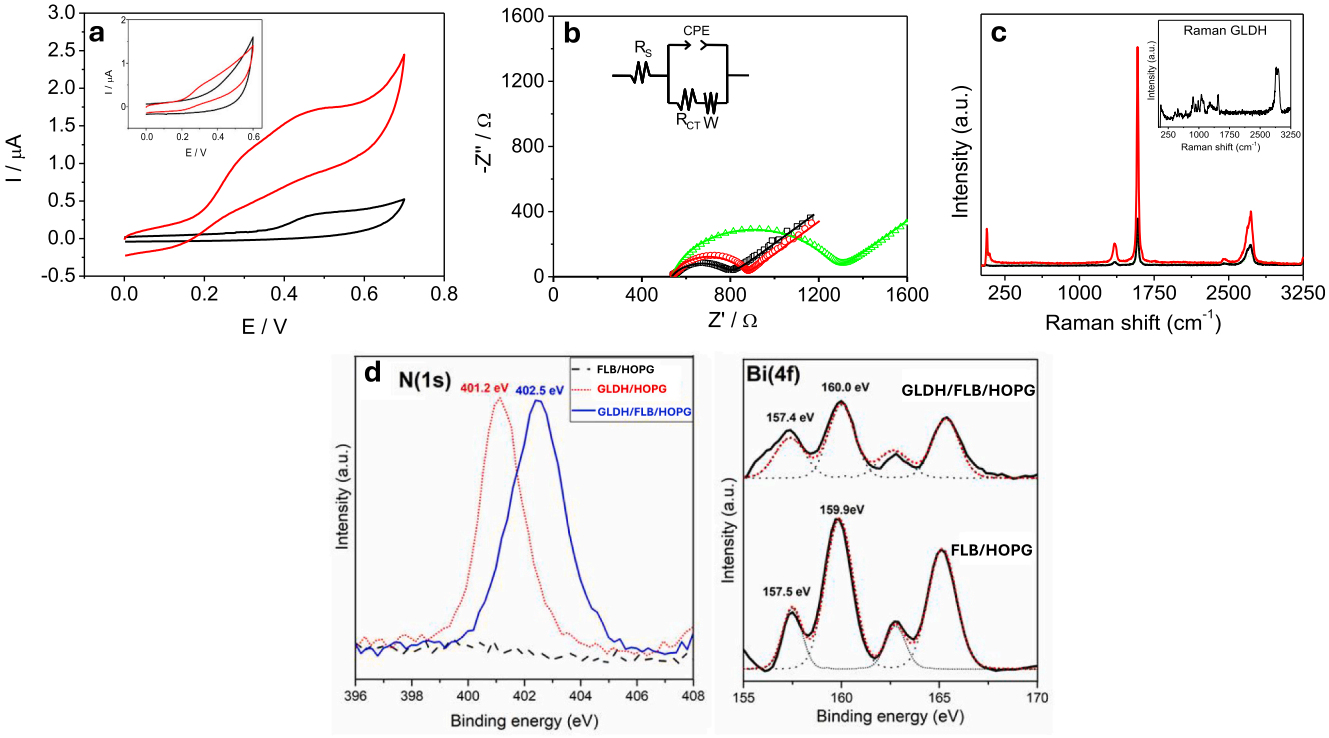

Fig. 2. (a) Cyclic voltammetric response of GLDH/FLB/SPGrE or GLDH/SPGrE (inset) biosensors in 0.1 M PB (pH 7.4) containing 10.0 mM NAD^+, before (black) and after (red) the addition of 1.0 mM glutamate. Scan rate: 0.01 V/s. (b) Nyquist diagrams obtained in 25 mM KCl in the presence of 10.0 mM $K_3Fe(CN)_6$/10.0 mM $K_4Fe(CN)_6$ for a bare SPGrE (black), FLB/SPGrE (red), GLDH/FLB/SPGrE (green). Inset: Electrical equivalent circuit. (c) Raman spectra of SPGrE (black), FLB/SPGrE (red), GLDH/FLB/SPGrE (green dotted). Inset: Raman spectra of GLDH. (d) XPS spectra of N(1s) for FLB/HOPG, GLDH/HOPG and GLDH/FLB/HOPG and Bi(4f) for FLB/HOPG and GLDH/FLB/HOPG. (For interpretation of the references to colour in this figure legend, the reader is referred to the web version of this article.)

analyze the FLB nanosheets. While bulk bismuth exhibits two main phonon peaks, E_g and A_{1g} modes at 71 cm^{-1} and 98 cm^{-1}, respectively [63], the single-point Raman spectrum of an FLB hexagon with a 5 nm thickness shows a blue shift of these bands, with the E_g mode at 83.3 cm^{-1} and the A_{1g} mode at 106.6 cm^{-1} (Fig. 1e). This observation is consistent with the previously reported thickness dependence of antimonene [64,65]. Additionally, a Raman spatial mapping of the A_{1g} mode was generated, revealing the same hexagonal morphology observed by other microscopy techniques (Fig. 1f). These results confirm the high crystallinity and two-dimensional aspect ratio of the FLB hexagons, highlighting their excellent structural quality.

3.2. Development of glutamate biosensor

The design of electrochemical biosensors that combine enzymes and nanomaterials is of great interest since these devices integrate, on the one hand, the catalytic properties of enzymes as well as their biorecognition capacity, as well as the excellent electronic properties of nanomaterials. In this context, 2D materials such as bismuthene exhibit highly attractive characteristics for the development of electrochemical enzymatic biosensors, including high surface area, good conductivity and biocompatibility.

To take advantage of these properties, FLB hexagons were deposited onto SPGrE (FLB/SPGrE) providing a stable and conductive platform for enzyme immobilization. Beyond its structural advantages, FLB plays a crucial role in enhancing the electrochemical properties of the electrode, facilitating the efficient oxidation of enzymatically generated NADH and acting as a mediator in the electrochemical process [58]. This is evident when studying the electrochemical behavior of FLB/SPGrE in the absence and presence of NADH (Fig. S5). In the absence of NADH, the cyclic voltammetric response of FLB/SPGrE exhibits a redox process corresponding to the oxidation of Bi^0 to Bi^{3+} (Fig. S5 inset). Upon the addition of 1.0 mM NADH, a significant increase in the anodic current is observed, starting at −0.1 V (Fig. S5, red) and reaching a peak potential at +0.18 V, with no corresponding cathodic peak, indicating pronounced electrocatalytic effect. Under the same conditions, NADH is also oxidized on unmodified SPGrE; however, in this case, the oxidation begins at +0.1 V, with the peak appearing at +0.39 V (Fig. S5, black). To demonstrate the feasibility of this approach, an amperometric biosensor for glutamate detection was developed by immobilizing GLDH on the FLB/SPGrE surface. The enzymatic reactions involved in the biosensing system are illustrated in Scheme 1. The enzyme catalyzes the oxidation of glutamate to α-ketoglutarate (1) while the cofactor NAD^+ is reduced to NADH (2), which in turn is oxidized back to NAD^+ at the FLB-modified electrode (3), producing an analytical signal proportional to the glutamate concentration. The cyclic voltammetric responses of the GLDH based biosensors in 0.1 M PB (pH 7.4) containing NAD^+ and glutamate are shown in Fig. 2a. In the absence of glutamate, both biosensors GLDH/SPGrE (Inset, black curve) and GLDH/FLB/SPGrE (black curve) exhibit a low current response, confirming that NAD^+ does not undergo significant redox activity in the studied potential range. However, in the presence of 1.0 mM glutamate, a noticeable electrocatalytic oxidation process is observed (red curves, Fig. 2a and inset), corresponding to the oxidation of the enzymatically generated NADH. Notably, the incorporation of FLB into the biosensor construction (red curve) results in a significant increase in the oxidation current and a slight shift in the onset potential compared to the response of GLDH/SPGrE (blue curve). The peak at +0.25 V observed in the red curve is likely associated with the electrocatalytic activity of FLB, which reduces the overpotential required for NADH oxidation, facilitating the oxidation of NADH enzymatically generated by GLDH at a lower potential. This behavior suggests that FLB facilitates electron transfer, most likely as a result of its electrocatalytic properties and enhanced charge transfer efficiency. These results highlight the beneficial role of FLB in improving

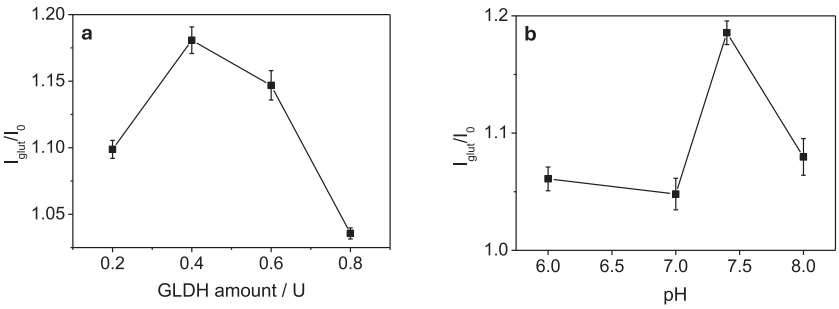

Fig. 3. (a) Dependence of the I_{glut}/I_0 with the different loadings of GLDH enzyme. (b) Effect of pH on the I_{glut}/I_0 ratio on a biosensor prepared with 0.4 U of GLDH. The data presented are the average value of three determinations.

the analytical performance of the biosensor, making it a promising material for the design of dehydrogenase-based biosensors and for the sensitive detection of relevant analytes.

The bioplatform was thoroughly characterized using various techniques to confirm the successful immobilization of the enzyme. EIS is a powerful tool for studying the interfacial properties of modified electrodes. To gain insight into how the modification process affects the conductivity and surface characteristics of the electrode, EIS experiments were performed at different functionalization stages. Fig. 2b shows the Nyquist plots corresponding to each modification stage obtained using a 25 mM KCl solution and 10.0 mM $K_3Fe(CN)_6/K_4Fe(CN)_6$ mixture. The impedance spectra were fitted using the Randles equivalent circuit shown in the inset in Fig. 2b, which comprises the following electronic elements: R_S, the electrolyte resistance between the working and reference electrodes; R_{CT}, the charge transfer resistance, and a constant phase element (CPE) that simulates the nonideal behavior of the capacitor associated with both the surface modification capacitance and double layer capacitance. In addition, a Warburg impedance (W) represents the delay that arises from diffusion of the electroactive species to the electrode. These results provide valuable in-sight into the changes in charge transfer resistance (R_{CT}), corresponding to the diameter of the semicircle, and interfacial behavior of the modified electrode. The bare SPGrE exhibits a relatively small semicircle, indicating low R_{CT} (271 Ω) which suggests good electron transfer at the electrode/electrolyte interface as expected for a graphene modified electrode. Upon modification with FLB, a significant increase in the semicircle diameter is observed. This increase can be attributed to the intrinsic conductivity of FLB. Unlike other 2D nanomaterials, FLB is less conductive and may present barriers to charge transfer. Despite this increase in R_{CT} (343 Ω), FLB primarily acts as a scaffold for enzyme immobilization. Further modification with GLDH results in a further high increase in charge transfer resistance (723 Ω), likely attributed to the less electroactive biolayer formed and therefore there are limitations to charge transfer associated with the presence of enzyme. To elucidate the role of FLB in enzyme immobilization, the electrochemical behavior of SPGrE modified solely with GLDH was also investigated by the same technique. When GLDH was directly immobilized onto the bare SPGrE, a large arc appeared in the Nyquist plot (Fig. S6). The semicircle is not fully developed at low frequencies, where a random dispersion of data points is observed. This result agrees well with an increase in the charge transfer resistance on the electrode surface, since the enzymatic layer forms an insulating barrier that limits the diffusion of the redox probe from the bulk solution to the electrode surface and hinders electron transfer, in agreement with the well-known poor electrical conductivity of most biomolecules. The Nyquist diagram clearly shows that the absence of FLB leads to a higher charge-transfer resistance, evidencing that FLB provides a conductive and biocompatible interface that facilitates enzyme immobilization while preserving favorable electrochemical properties. In this case, the impedance data corresponding to the GLDH/SPGrE were fitted using the equivalent circuit shown in Fig. S6. The experimental results and those obtained from the fitting (Table S1) confirm successful and stepwise modification of the electrode and demonstrate the feasibility of enzymatic immobilization on FLB for the designing of electrochemical enzymatic biosensor.

The Raman spectra of FLB/SPGrE and GLDH/FLB/SPGrE (Fig. 2c) exhibit two characteristic bands at 69 and 97 cm^{-1}, attributed to the E_g in-plane vibrational mode and the A_{1g} out-of-plane mode of metallic bismuth, respectively [63]. The remaining bands in the spectra are attributed to graphene. In particular, the band at approximately 1356 cm^{-1} (D-band) corresponds to the defects caused by sp^3 hybridized carbons in the graphene, while the band at 1590 cm^{-1} (G-band) is characteristic of the graphite domains of sp^2 bonded carbon present in the graphene lattice structure [66]. The Raman spectrum of GLDH (Fig. 2c inset) exhibits characteristic bands corresponding to specific vibrational modes of protein structure. In particular, the region between 800 and 1100 cm^{-1} contains peaks associated with aromatic amino acid residues, such as tyrosine and phenylalanine, which are commonly observed in protein spectra. The band at 1462 cm^{-1} corresponds to C—H bending and N—H deformation modes, while the peaks located at 2900 and 2938 cm^{-1} are assigned to C—H stretching vibrations from aliphatic chains in the protein backbone [67]. The presence of these peaks in the Raman spectrum of GLDH/FLB/SPGrE provides strong evidence of the successful immobilization of GLDH onto the modified electrode surface without protein denaturation or structural alterations that could compromise the enzymatic activity.

Fig. 2d (left side) shows the XPS spectra of N(1s) which confirm the presence of this element in both electrode samples where GLDH was immobilized (red and blue spectra), and the absence of this signal for the FLB/HOPG electrode (black spectrum), as expected. The best fit of the N (1 s) core level shows only one contribution at 401.2 eV binding energy for the GLDH/HOPG assigned to graphitic N. In contrast, the GLDH/FLB/HOPG electrode exhibits a peak at 402.5 eV binding energy attributed to oxidized nitrogen species, confirming the different interaction if the GLDH enzyme is immobilized on FLB/HOPG instead of directly on HOPG electrode. The incorporation of the FLB on the electrode surface can be easily confirmed by the appearance of the two peaks due to the Bi 4f splitting (see Fig. 2d on the right). For the FLB/HOPG electrode, regarding the Bi 4f region, the valence state of Bi^0 is confirmed by observing a component centred at 157.5 eV, which can be identified as Bi $4f_{7/2}$ signal of Bi^0 [68]. In addition, a second component at 159.9 eV assigned to Bi_2O_3 is also observed. Therefore, the spectrum shows the presence of metallic Bi (at 157.5 eV BE) and oxidized Bi (at 159.9 eV BE) assigned to Bi_2O_3 [69]. In the case of the GLDH/FLB/HOPG electrode, both components are also observed at 157.4 and 160.0 eV, the first component increases from 21.8% (FLB/HOPG) in the previous case to 36.8% (GLDH/FLB/HOPG), due to the extra contribution of the Bi—N assignment which overlaps in the same region as the Bi^0 assignment, thus confirming the presence of the GLDH enzyme.

The morphology of the surface modified with the GLDH enzyme was studied by AFM. The topographic AFM image of GLDH/FLB (Fig. S7) provides clear evidence of enzyme presence on the FLB-modified surface. The surface is covered with a film composed of enzyme-associated

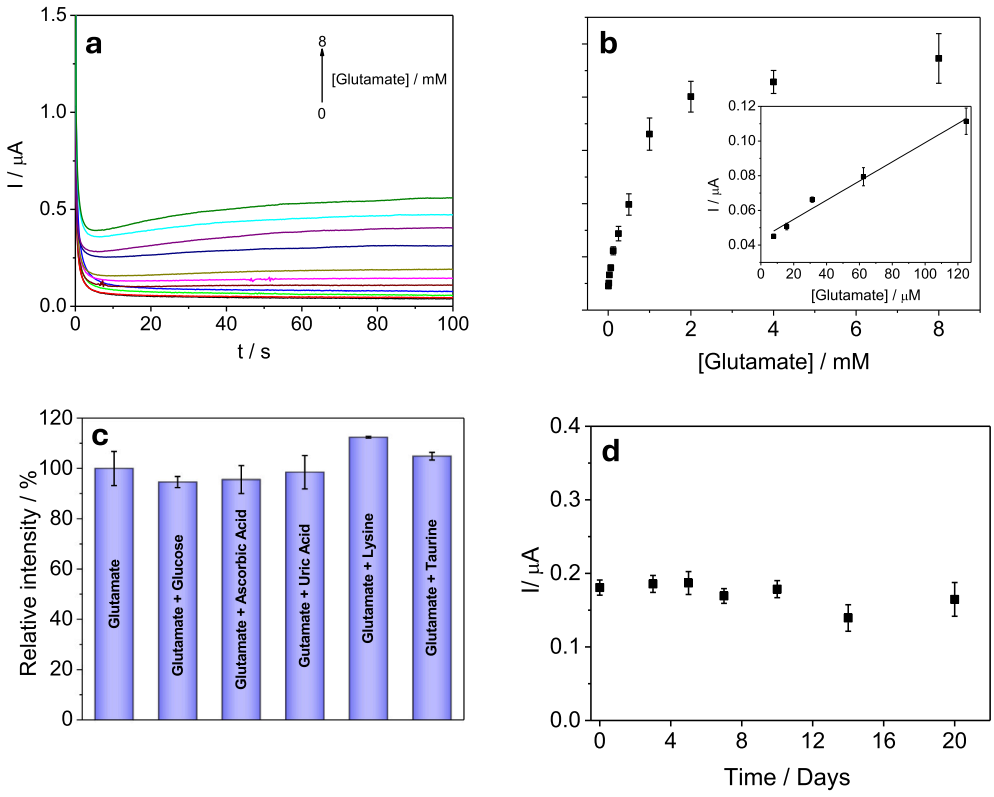

Fig. 4. (a) Chronoamperometric responses (E_{ap} = +0.2 V) of the biosensor (GLDH/FLB/SPGrE) in 0.1 M PB (pH 7.4) containing 10.0 mM NAD^+ after the addition of increasing amounts of glutamate. (b) Calibration curve obtained from the chronoamperometric currents *vs* glutamate concentration. The inset shows the linear concentration range. (c) Relative response of the biosensor to 0.10 mM glutamate measured in the presence of potentially interfering compounds at the concentration of 0.10 mM. (d) Amperometric responses of GLDH/FLB/SPGrE in 0.1 M PB (pH 7.4) containing 10.0 mM NAD^+ and 0.5 mM glutamate for 20 days. The data presented are the average value of three determinations.

globules distributed across the surface, interspersed with uncoated regions. The average height of approximately 6 nm is consistent with the expected size [70,71], suggesting that the surface is nearly monolayered.

Collectively, these results, from various characterization techniques, confirm the successful modification of the SPGrE with FLB and GLDH, supporting the development of a dehydrogenase-based biosensor.

3.3. Amperometric response of GLDH/FLB/SPGrE glutamate biosensor

The glutamate sensing property of the biosensor was evaluated by chronoamperometry. The amount of enzyme used in its development was optimized to achieve optimal analytical performance. For this purpose, biosensors incorporating increasing amounts of GLDH were prepared, and their chronoamperometric responses at +0.2 V were recorded both in the absence (I_0) and presence of 0.5 mM glutamate and 10.0 mM NAD^+ (I_{glut}) (Fig. 3a). The I_{glut}/I_0 ratio increased as the enzyme loading in the biosensing layer was raised, reaching a maximum at 0.4 U. Beyond this concentration, a decrease in the I_{glut}/I_0 ratio was observed, indicating that an excessive enzyme load on FLB/SPGrE could hinder charge transfer to the electrode surface. Consequently, 0.4 U was selected as the optimal enzyme amount. Additionally, the influence of the buffer solution pH (ranging from 6.0 to 8.0) on the biosensor chronoamperometric response was investigated (Fig. S8). The I_{glut}/I_0 ratio increased with pH, peaking at 7.4 before decreasing (Fig. 3b). Based on these results, all subsequent electrochemical measurements were carried out in 0.1 M PB at pH 7.4.

Under these optimal conditions, the chronoamperometric response at +0.2 V of the biosensor in the presence of glutamate was investigated. Fig. 4a shows that the current response of GLDH/FLB/SPGrE biosensor to glutamate increased with increasing glutamate concentration, and Fig. 4b depicts the calibration curve between current and glutamate concentration in the presence of 10.0 mM NAD^+ in 0.1 M PB (pH 7.4), which follows Michaelis-Menten kinetics. This confirms that the analytical response is controlled by the enzymatic reaction. The Michaelis–Menten constant (K_M) was estimated to be 0.66 ± 0.07 mM from the Lineweaver–Burk plot (Fig. S9), using the Lineweaver–Burk eq. $1/I = (K_M/V_{max})(1/[\text{Glutamate}]) + 1/V_{max}$. Fitting the experimental data to the linear eq. $1/I = 1.29 \pm 0.09\,(1/[Glutamate]) + 2.0 \pm 0.2$ gave a V_{max} of 0.51 ± 0.04 μA. The obtained $K_M$value is lower or similar to those reported for other GLDH–nanomaterial modified electrodes [72–74], indicating a comparable substrate affinity. As expected, the value of K_M obtained is higher than that obtained for the free enzyme, which has been estimated at 0.47 mM. This result indicates that GLDH retains its great affinity to glutamate after being deposited into the FLBs. The analytical properties of the biosensor were obtained from the linear part (up to 125 μM, $R^2 = 0.990$) of the calibration plot. In this part, the chronoamperometric response and the glutamate concentration fit to the next equation: I (μA) = (0.55 ± 0.04) [glutamate] (mM) + (0.043 ± 0.002) (inset Fig. 4b). Data presented are the average value of three determinations. The sensitivity calculated from the slope of the plot was found to be 0.55 ± 0.04 μA mM^{-1}, which was a 42% improvement over GLDH/SPGrE (Fig. S10). The limits of detection (LOD) and quantification (LOQ) were calculated from the slope of the plot and found to be 1.96 μM and 6.54 μM, respectively, based on a signal-to-noise ratio of 3 (S/N = 3).

A detailed comparison of the analytical parameters (Table S2) reveals that the FLB/SPGrE biosensor combines favorable working potential, linear range, and detection limit compared with previously reported GLDH-based systems. The operating potential of +0.2 V (*vs* Ag pseudo-reference) is similar or lower than that required by most enzymatic electrodes and considerably lower than those operating between

Table 1
Determination of glutamate in different samples with the GLDH biosensor and with a commercial enzymatic assay kit.

	GLDH Biosensor	Enzymatic kit		GLDH Biosensor		
	Found/mg/g	Found/mg/g		Added/μM	Found/μM	Recovery/%
Chicken bouillon cubes	207 ± 16	203 ± 13	Human serum	20	19 ± 2	95
				50	55 ± 2	109
				100	95 ± 4	95

+0.4 and + 0.5 V, which minimizes possible interferences and enhances selectivity. Its linear range (6.54–125 μM) is also consistent with the concentration levels of glutamate typically found in biological samples [21], and comparable to those achieved with other nanostructured electrodes such as carbon nanotubes or graphene-based systems. It is noteworthy that the detection limit of 1.96 μM obtained for the FLB/SPGrE biosensor is comparable to or lower than those reported in the literature, being the lowest recorded for enzymatic biosensors using screen-printed electrodes, confirming the beneficial effect of few-layer bismuthene in promoting efficient electron transfer and enhanced catalytic performance. These results underscore the excellent analytical performance of the proposed biosensor for glutamate determination in real samples.

In addition, the repeatability and reproducibility of the proposed biosensor were evaluated. Repeatability was first assessed by recording the biosensor response to 0.10 mM glutamate ten consecutive times using the same bioplatform, yielding a relative standard deviation (RSD) of 5%. Additionally, the reproducibility was evaluated by comparing the analytical signals from ten different biosensors prepared in the same manner whose value obtained is less than 7%. Regarding storage stability, the GLDH/FLB/SPGrE biosensor stored at 4 °C under light- and humidity-free conditions exhibits a highly consistent response in 0.5 mM glutamate solutions for at least 20 days. During this period, it retains 90% of its initial signal, as illustrated in Fig. 4d, thereby demonstrating its reliability over time.

Selectivity is a key factor in the design of enzymatic biosensors intended for the analysis of biological or food samples. To evaluate this parameter, the influence of potential interfering compounds on the biosensor response was investigated. Fig. 4c shows the relative response, expressed as the ratio of the biosensor signals recorded for 0.10 mM glutamate in the absence and in the presence of various potential interferent compounds, including glucose, ascorbic acid, uric acid, lysine, and taurine, which are commonly found in such samples. The results indicate that none of these substances significantly affect the biosensor response when tested at the same concentration as the target analyte (0.1 mM). To ensure that the biosensor response is specific to glutamate, an interference study was also carried out in the presence of high concentration (0.50 mM) of potential interfering compounds. Results clearly showed no effects of the potential interfering compounds on the biosensor response (see Fig. S11) even at high concentrations, indicating the high selectivity of the developed biosensor. These findings confirm that the GLDH/FLB/SPGrE biosensor enables the selective detection of glutamate.

3.4. Determination of glutamate in food and clinical samples

The developed biosensor was applied to the direct determination of glutamate in both food and clinical samples using the standard addition method. Specifically, glutamate determination in chicken bouillon cubes was performed after analyte extraction as described in the Experimental section. The results obtained with the biosensor were compared with those achieved by a commercial enzymatic assay, and the corresponding data are summarized in Table 1. The average glutamate concentration obtained for three measurements using different biosensors showed good agreement with that obtained using the commercial enzymatic kit and the statistical analysis of comparison of the experimental mean of both methods confirms that there is no significant difference between the two methods at the 5% level, since values of t were less than the critical value.

On the other hand, a recovery study of glutamate in human serum was conducted. For this purpose, the recoveries obtained by triplicated analysis were evaluated by spiking the serum diluted 100-fold with several known amounts of analyte (20.0, 50.0 and 100 μM). The results are presented in Table 1. As can be observed, good recoveries were obtained in all cases. These results demonstrate that the design of bioplatforms based on the use of FLB as a redox mediator and dehydrogenase enzyme is a suitable approach for the determination of glutamate in different types of samples.

4. Conclusions

A novel enzymatic electrochemical biosensor for glutamate detection was developed by integrating few-layer bismuthene (FLB) onto screen-printed graphene electrodes. Morphological and spectroscopic characterization confirmed the successful synthesis of FLB and its stable deposition on the electrode surface. Electrochemical studies demonstrated that FLB, acting as a redox mediator, significantly enhances the analytical performance of the biosensor, enabling a wide linear detection range (6.54–125 μM) and a low detection limit (1.96 μM). The biosensor exhibited high reproducibility (<7% RSD) and stability, retaining 90% of its initial response after 20 days of storage. Selectivity tests confirmed that common interfering compounds did not significantly affect the biosensor signal. The platform was successfully applied to the quantification of glutamate in real samples, achieving good recoveries at different concentration levels in human serum and accurate results in food analysis, comparable to a commercial enzymatic assay. These results highlight the suitability of FLB as a functional nanomaterial for dehydrogenase-based biosensing applications, offering a promising alternative to classical methods for glutamate detection in clinical diagnostics and food safety monitoring.

CRediT authorship contribution statement

Ana María Villa-Manso: Investigation, Data curation. **Iñigo Torres:** Investigation, Data curation. **Félix Pariente:** Writing – original draft. **Encarnación Lorenzo:** Writing – original draft, Supervision. **Félix Zamora:** Writing – original draft, Supervision. **Eva Mateo-Martí:** Investigation, Data curation. **Cristina Gutiérrez-Sánchez:** Writing – original draft, Supervision, Funding acquisition. **Mónica Revenga-Parra:** Writing – original draft, Supervision, Funding acquisition.

Declaration of competing interest

The authors declare that they have no known competing financial interests or personal relationships that could have appeared to influence the work reported in this paper.

Acknowledgements

This work has been supported by the Spanish Ministerio de Ciencia, Innovación y Universidades (TED2021–129738B-I00, PID2022-142262OA-I00, PID2023-1508440B-I00 and RED2022-134120-T).

Appendix A. Supplementary data

Supplementary data to this article can be found online at https://doi.org/10.1016/j.microc.2026.117286.

Data availability

Data will be made available on request.

References

[1] A. Gasbarri, A. Pompili, Involvement of glutamate in learning and memory, in: A. Meneses (Ed.), Identification of Neural Markers Accompanying Memory, Elsevier, 2014, pp. 63–77, https://doi.org/10.1016/B978-0-12-408139-0.00004-3.

[2] L.C. Jansson, K.E. Åkerman, The role of glutamate and its receptors in the proliferation, migration, differentiation and survival of neural progenitor cells, J. Neural Transm. 121 (2014) 819–836, https://doi.org/10.1007/s00702-014-1174-6.

[3] Y. Uno, J.T. Coyle, Glutamate hypothesis in schizophrenia, Psychiatry Clin. Neurosci. 73 (2019) 204–215, https://doi.org/10.1111/pcn.12823.

[4] S. Nisar, A.A. Bhat, T. Masoodi, S. Hashem, S. Akhtar, T.A. Ali, S. Amjad, S. Chawla, P. Bagga, M.P. Frenneaux, Genetics of glutamate and its receptors in autism spectrum disorder, Mol. Psychiatry 27 (2022) 2380–2392, https://doi.org/10.1038/s41380-022-01506-w.

[5] F.J. Arnold, A.F. Putka, U. Raychaudhuri, S. Hsu, R.S. Bedlack, C.L. Bennett, A. R. La Spada, Revisiting glutamate excitotoxicity in amyotrophic lateral sclerosis and age-related neurodegeneration, Int. J. Mol. Sci. 25 (2024) 5587, https://doi.org/10.3390/ijms25115587.

[6] V.N. Bukke, M. Archana, R. Villani, A.D. Romano, A. Wawrzyniak, K. Balawender, S. Orkisz, S. Beggiato, G. Serviddio, T. Cassano, The dual role of glutamatergic neurotransmission in Alzheimer's disease: from pathophysiology to pharmacotherapy, Int.J.Mol.Sci. 21 (2020) 7452, https://doi.org/10.3390/ijms21207452.

[7] L. Iovino, M.E. Tremblay, L. Civiero, Glutamate-induced excitotoxicity in Parkinson's disease: the role of glial cells, J.Pharmacol.Sci. 144 (2020) 151–164, https://doi.org/10.1016/j.jphs.2020.07.011.

[8] J. Du, X. Li, Y. Li, Glutamate in peripheral organs: biology and pharmacology, Eur. J. Pharmacol. 784 (2016) 42–48, https://doi.org/10.1016/j.ejphar.2016.05.009.

[9] K. Kurihara, Glutamate: from discovery as a food flavor to role as a basic taste (umami), Am. J. Clin. Nutr. 90 (3) (2009) 719S–722S, https://doi.org/10.3945/ajcn.2009.27462D.

[10] A. Zanfirescu, A. Ungurianu, A.M. Tsatsakis, G.M. Nițulescu, D. Kouretas, A. Veskoukis, D. Tsoukalas, A.B. Engin, M. Aschner, D. Margină, A review of the alleged health hazards of monosodium glutamate, Compr. Rev. Food Sci. Food Saf. 18 (2019) 1111–1134, https://doi.org/10.1111/1541-4337.12448.

[11] R. Walker, J.R. Lupien, The safety evaluation of monosodium glutamate, J. Nutr. 130 (4) (2000) 1049S–1052S, https://doi.org/10.1093/jn/130.4.1049S.

[12] EFSA Panel on Food Additives and Nutrient Sources added to Food (ANS), A. Mortensen, F. Aguilar, R. Crebelli, A. Di Domenico, B. Dusemund, M.J. Frutos, P. Galtier, D. Gott, U. Gundert-Remy, J. Leblanc, O. Lindtner, P. Moldeus, P. Mosesso, D. Parent-Massin, A. Oskarsson, I. Stankovic, I. Waalkens-Berendsen, R. A. Woutersen, M. Wright, M. Younes, P. Boon, D. Chrysafidis, R. Gürtler, P. Tobback, A. Altieri, A.M. Rincon, C. Lambré, Re-evaluation of glutamic acid (E 620), sodium glutamate (E 621), potassium glutamate (E 622), calcium glutamate (E 623), ammonium glutamate (E 624) and magnesium glutamate (E 625) as food additives, EFSA J. 15 (2017) e04910, https://doi.org/10.2903/j.efsa.2017.4910.

[13] Y. Katrancı, A. Aydemir, B. Kızılkaya, G.Y. Baştemur, S.P. Ozkorucuklu, Investigation of monosodium glutamate content in flavors, seasonings, and sauces from local markets in Turkey, Food Sci. Nutr. 12 (2024) 7806–7813, https://doi.org/10.1002/fsn3.4406.

[14] T. Populin, S. Moret, S. Truant, L.S. Conte, A survey on the presence of free glutamic acid in foodstuffs, with and without added monosodium glutamate, Food Chem. 104 (2007) 1712–1717, https://doi.org/10.1016/j.foodchem.2007.03.034.

[15] T. Nuzzo, A. Mancini, M. Miroballo, A. Casamassa, A. Di Maio, G. Donati, G. Sansone, L. Gaetani, F.P. Paoletti, A. Isidori, P. Calabresi, F. Errico, L. Parnetti, A. Usiello, High performance liquid chromatography determination of l-glutamate, l-glutamine and glycine content in brain, cerebrospinal fluid and blood serum of patients affected by Alzheimer's disease, Amino Acids 53 (2021) 435–449, https://doi.org/10.1007/s00726-021-02943-7.

[16] M. Soyseven, H. Aboul-Enein, G. Arli, Development of a HPLC method combined with ultraviolet/diode array detection for determination of monosodium glutamate in various food samples, Int. J. Food Sci. Technol. 56 (2021) 461–467, https://doi.org/10.1111/ijfs.14661.

[17] C.D.M. Campos, P.A. de Campos Braga, F.G.R. Reyes, J.A.F. da Silva, Elimination of the artefact peaks in capillary electrophoresis determination of glutamate by using organic solvents in sample preparation, J. Sep. Sci. 38 (2015) 3781–3787, https://doi.org/10.1002/jssc.201500601.

[18] H.M. Ali, S.F. Hammad, S. El-Malla, Green spectrophotometric methods for determination of a monosodium glutamate in different matrices, Microchem. J. 169 (2021) 106622, https://doi.org/10.1016/j.microc.2021.106622.

[19] A. Bedair, R.M. Abdelhameed, S.F. Hammad, I.A. Abdallah, M. Locatelli, F. R. Mansour, A luminescent metal-organic framework composite as a turn-on sensor for the selective determination of monosodium glutamate in instant noodles, Microchem. J. 204 (2024) 111132, https://doi.org/10.1016/j.microc.2024.111132.

[20] Z. Jiao, X. Jiang, S. Hou, M. Tang, B. Zhao, Highly sensitive and selective luminescence sensor based on two-fold interpenetrated MOFs for detecting glutamate in serum, Inorg. Chem. 59 (2020) 2171–2177, https://doi.org/10.1021/acs.inorgchem.9b02752.

[21] J. Schultz, Z. Uddin, G. Singh, M.M. Howlader, Glutamate sensing in biofluids: recent advances and research challenges of electrochemical sensors, Analyst 145 (2020) 321–347, https://doi.org/10.1039/C9AN01609K.

[22] L. Zhong, Z. Wang, X. Ye, J. Cui, Z. Wang, S. Jia, Molecular simulations guide immobilization of lipase on nest-like ZIFs with regulatable hydrophilic/hydrophobic surface, J. Colloid Interface Sci. 667 (2024) 199–211, https://doi.org/10.1016/j.jcis.2024.04.075.

[23] L. Zhong, Y. Feng, Z. Wang, T. Tian, Y. Bi, J. Cui, Immobilized lipase on MIL-53 (Al)-AM11 with regulatable hydrophobic surface for flavor ester synthesis, Int. J. Biol. Macromol. 305 (2025) 141322, https://doi.org/10.1016/j.ijbiomac.2025.141322.

[24] C. Gutiérrez-Sánchez, D. Olea, M. Marques, V.M. Fernández, I.A.C. Pereira, M. Vélez, A.L. De Lacey, Oriented immobilization of a membrane-bound hydrogenase onto an electrode for direct electron transfer, Langmuir 27 (2011) 6449–6457, https://doi.org/10.1021/la200141t.

[25] G. García-Molina, P. Natale, L. Valenzuela, J. Alvarez-Malmagro, C. Gutiérrez-Sánchez, A. Iglesias-Juez, I. López-Montero, M. Vélez, M. Pita, A. De Lacey .L., Potentiometric detection of ATP based on the transmembrane proton gradient generated by ATPase reconstituted on a gold electrode, Bioelectrochemistry 133 (2020) 107490, https://doi.org/10.1016/j.bioelechem.2020.107490.

[26] C. Gutiérrez-Sánchez, M. Pita, C. Vaz-Domínguez, S. Shleev, A.L. De Lacey, Gold nanoparticles as electronic bridges for laccase-based biocathodes, J. Am. Chem. Soc. 134 (2012) 17212–17220, https://doi.org/10.1021/ja307308j.

[27] Y. Du, L. Zhao, Z. Geng, Z. Huo, H. Li, X. Shen, X. Peng, R. Yan, J. Cui, S. Jia, Construction of catalase@hollow silica nanosphere: catalase with immobilized but not rigid state for improving catalytic performances, Int. J. Biol. Macromol. 263 (2024) 130381, https://doi.org/10.1016/j.ijbiomac.2024.130381.

[28] I. Bravo, M. Revenga-Parra, F. Pariente, E. Lorenzo, Reagent-less and robust biosensor for direct determination of lactate in food samples, Sensors (Basel, Switzerland) 17 (2017) 144, https://doi.org/10.3390/s17010144.

[29] H. Hu, Y. Chang, Z. Wang, J. Cui, S. Jia, Y. Du, A chemo-biocatalyst based on glutamate oxidase-integrated biomimetic trimanganese tetraoxide as cascade composite nano-catalyst for synthesis of α ketoglutaric acid, J. Colloid Interface Sci. 650 (2023) 1833–1841, https://doi.org/10.1016/j.jcis.2023.07.137.

[30] Y. Du, X. Luo, X. Ye, M. Song, Y. Li, S. Yang, C. Huang, J. Cui, Molecular imprinted photoresponse hybrid biocatalyst for ultrasensitive glutamate detection, Int. J. Biol. Macromol. 308 (2025) 142540, https://doi.org/10.1016/j.ijbiomac.2025.142540.

[31] P. Li, J. Jia, Z. Geng, S. Pang, R. Wang, M. Bilal, H. Bian, J. Cui, S. Jia, A dual enzyme-phosphate hybrid nanoflower for glutamate detection, Particuology 83 (2023) 63–70, https://doi.org/10.1016/j.partic.2023.02.008.

[32] H. Jaegfeldt, 420 - a study of the products formed in the electrochemical reduction of nicotinamide-adenine-dinucleotide, Bioelectrochem. Bioenerg. 8 (1981) 355–370, https://doi.org/10.1016/0302-4598(81)80018-9.

[33] J. Moiroux, P.J. Elving, Effects of adsorption, electrode material, and operational variables on the oxidation of dihydronicotinamide adenine dinucleotide at carbon electrodes, Anal. Chem. 50 (1978) 1056–1062, https://doi.org/10.1021/ac50030a015.

[34] M. Wang, X. Kan, Multilayer sensing platform: gold nanoparticles/prussian blue decorated graphite paper for NADH and H2O2 detection, Analyst 143 (2018) 5278–5284, https://doi.org/10.1039/C8AN01502C.

[35] H. Yu, Z. Ma, Z. Wu, Immobilization of Ni-pd/core-shell nanoparticles through thermal polymerization of acrylamide on glassy carbon electrode for highly stable and sensitive glutamate detection, Anal. Chim. Acta 896 (2015) 137–142, https://doi.org/10.1016/j.aca.2015.09.005.

[36] T. Gurusamy, R. Rajaram, G.R. Kandregula, K. Ramanujam, Electrochemical sensing of NADH using 4-nitrobenzenediazonium tetrafluoroborate salt functionalized multiwalled carbon nanotubes, Dalton Trans. 52 (2023) 641–651, https://doi.org/10.1039/D3DT00216K.

[37] T. Rębiś, M. Kuznowicz, A. Jędrzak, G. Milczarek, T. Jesionowski, Design and fabrication of low potential NADH-sensor based on poly(caffeic acid)@multi-walled carbon nanotubes, Electrochim. Acta 386 (2021) 138384, https://doi.org/10.1016/j.electacta.2021.138384.

[38] M. Revenga-Parra, A. Villa-Manso, M. Briones, E. Mateo-Martí, E. Martínez-Periñán, E. Lorenzo, F. Pariente, Bioelectrocatalytic platforms based on chemically modified nanodiamonds by diazonium salt chemistry, Electrochim. Acta 357 (2020) 136876, https://doi.org/10.1016/j.electacta.2020.136876.

[39] X. Li, X. Kan, A boronic acid carbon nanodots/poly(thionine) sensing platform for the accurate and reliable detection of NADH, Bioelectrochemistry 130 (2019) 107344, https://doi.org/10.1016/j.bioelechem.2019.107344.

[40] E. Martínez-Periñán, A. Domínguez-Saldaña, A. Villa-Manso, C. Gutiérrez-Sánchez, M. Revenga-Parra, E. Mateo-Martí, F. Pariente, E. Lorenzo, Azure a embedded in carbon dots as NADH electrocatalyst: development of a glutamate electrochemical biosensor, Sens. Actuat. B Chem. 374 (2023) 132761, https://doi.org/10.1016/j.snb.2022.132761.

[41] N. Baig, Two-dimensional nanomaterials: a critical review of recent progress, properties, applications, and future directions, Compos. A: Appl. Sci. Manuf. 165 (2023) 107362, https://doi.org/10.1016/j.compositesa.2022.107362.

[42] C. Deepa, L. Rajeshkumar, M. Ramesh, Preparation, synthesis, properties and characterization of graphene-based 2D nanomaterials for biosensors and

bioelectronics, Mater.Res.Techno. 19 (2022) 2657–2694, https://doi.org/10.1016/j.jmrt.2022.06.023.
[43] S. Tajik, Z. Dourandish, F. Garkani Nejad, H. Beitollahi, P.M. Jahani, A. Di Bartolomeo, Transition metal dichalcogenides: synthesis and use in the development of electrochemical sensors and biosensors, Biosens. Bioelectron. 216 (2022) 114674, https://doi.org/10.1016/j.bios.2022.114674.
[44] N.R. Glavin, R. Rao, V. Varshney, E. Bianco, A. Apte, A. Roy, E. Ringe, P.M. Ajayan, Emerging applications of elemental 2D materials, Adv. Mater. 32 (2020) 1904302, https://doi.org/10.1002/adma.201904302.
[45] T. García-Mendiola, C. Gutiérrez-Sánchez, C. Gibaja, I. Torres, C. Busó-Rogero, F. Pariente, J. Solera, Z. Razavifar, J.J. Palacios, F. Zamora, E. Lorenzo, Functionalization of a few-layer Antimonene with oligonucleotides for DNA sensing, ACS Appl. Nano Mater. 3 (2020) 3625–3633, https://doi.org/10.1021/acsanm.0c00335.
[46] Y. Zhang, Y. Xu, N. Li, X. Liu, Y. Ma, SiyiYang, H. Luo, C. Hou, D. Huo, An ultrasensitive electrochemical sensor based on antimonene simultaneously detect multiple heavy metal ions in food samples, Food Chem. 421 (2023) 136131, https://doi.org/10.1016/j.foodchem.2023.136131.
[47] H. Li, Z. Yang, Recent Progress in synthesis and photonic applications of two-dimensional Bismuthene, Appl.Sci. 13 (2023) 6885, https://doi.org/10.3390/app13126885.
[48] P. Sujita, S. Vadivel, S. Wacławek, B. Paul, Few layers of bismuthene as an ideal material for electrochemical applications: a review, Inorg.Chem. Commun. 167 (2024) 112739, https://doi.org/10.1016/j.inoche.2024.112739.
[49] K.O. Adeniyi, G. Manavalan, A. Zainelabdin, J. Mikkola, S. Tesfalidet, Solution-processable Bismuthene nanosheets for ultrasensitive sensing of heavy metal ions via anodic stripping voltammetry, ACS Appl. Nano Mater. 7 (2024) 20217–20228, https://doi.org/10.1021/acsanm.4c03008.
[50] A.C. Lazanas, K. Tsirka, A.S. Paipetis, M.I. Prodromidis, 2D bismuthene/graphene modified electrodes for the ultra-sensitive stripping voltammetric determination of lead and cadmium, Electrochim. Acta 336 (2020) 135726, https://doi.org/10.1016/j.electacta.2020.135726.
[51] M.A. Tapia, C. Pérez-Ràfols, R. Gusmão, N. Serrano, Z. Sofer, J. Díaz-Cruz .M., Enhanced voltammetric determination of metal ions by using a bismuthene-modified screen-printed electrode, Electrochim. Acta 362 (2020) 137144, https://doi.org/10.1016/j.electacta.2020.137144.
[52] Y. Zhang, Y. Qin, L. Jiao, H. Wang, Z. Wu, X. Wei, Y. Wu, N. Wu, L. Hu, H. Zhong, W. Gu, C. Zhu, Atomically thin bismuthene nanosheets for sensitive electrochemical determination of heavy metal ions, Anal. Chim. Acta 1235 (2022) 340510, https://doi.org/10.1016/j.aca.2022.340510.
[53] L. Gutiérrez-Gálvez, D. García-Fernández, M. Barrio, M. Luna, Í. Torres, F. Zamora, C. Navío, P. Milán-Rois, M. Castellanos, M. Abreu, R. Cantón, J.C. Galán, Á. Somoza, R. Miranda, T. García-Mendiola, E. Lorenzo, Free PCR virus detection via few-layer bismuthene and tetrahedral DNA nanostructured assemblies, Talanta 269 (2024) 125405, https://doi.org/10.1016/j.talanta.2023.125405.
[54] E. Enebral-Romero, D. García-Fernández, L. Gutiérrez-Gálvez, D. López-Diego, M. Luna, A. García-Martín, E. Salagre, E.G. Michel, Í. Torres, F. Zamora, T. García-Mendiola, E. Lorenzo, Bismuthene - tetrahedral DNA nanobioconjugate for virus detection, Biosens. Bioelectron. 261 (2024) 116500, https://doi.org/10.1016/j.bios.2024.116500.
[55] L. Gutiérrez-Gálvez, E. Enebral-Romero, M.Á. Valle Amores, C. Pina Coronado, I. Torres, D. López-Diego, M. Luna, A. Fraile, F. Zamora, J. Alemán, J. Álvarez, M. J. Capitán, E. Lorenzo, T. García-Mendiola, Advancing diagnostics with BODIPY-bismuthene DNA biosensors, Nanoscale 17 (2025) 8126–8140, https://doi.org/10.1039/D4NR05258G.
[56] C. Mayorga-Martinez, R. Gusmão, Z. Sofer, M. Pumera, Pnictogen-based enzymatic phenol biosensors: phosphorene, arsenene, antimonene, and bismuthene, Angew. Chem. Int. Ed. 58 (2019) 134–138, https://doi.org/10.1002/anie.201808846.
[57] H.L. Chia, C. Mayorga-Martinez, R. Gusmão, F. Novotny, R.D. Webster, M. Pumera, A highly sensitive enzyme-less glucose sensor based on pnictogens and silver shell-gold core nanorod composites, Chem. Commun. 56 (2020) 7992–7995, https://doi.org/10.1039/D0CC02770G.
[58] I. Torres, A. Villa-Manso, M. Revenga-Parra, C. Gutiérrez-Sánchez, D.A. Aldave, E. Salagre, E.G. Michel, M. Varela, J. Gómez-Herrero, E. Lorenzo, F. Pariente, F. Zamora, Preparation of high-quality few-layers bismuthene hexagons, Appl. Mater. Today 26 (2022) 101360, https://doi.org/10.1016/j.apmt.2021.101360.
[59] A. Gimeno, P. Ares, I. Horcas, A. Gil, J.M. Gómez-Rodríguez, J. Colchero, J. Gómez-Herrero, 'Flatten plus': a recent implementation in WSxM for biological research, Bioinformatics 31 (2015) 2918–2920, https://doi.org/10.1093/bioinformatics/btv278.
[60] I. Horcas, R. Fernández, J.M. Gómez-Rodríguez, J. Colchero, J. Gómez-Herrero, A. M. Baro, WSXM: a software for scanning probe microscopy and a tool for nanotechnology, Rev. Sci. Instrum. 78 (2007) 013705, https://doi.org/10.1063/1.2432410.
[61] P. Nemes-Incze, Z. Osváth, K. Kamarás, L. Biró P., Anomalies in thickness measurements of graphene and few layer graphite crystals by tapping mode atomic force microscopy, Carbon 46 (2008) 1435–1442, https://doi.org/10.1016/j.carbon.2008.06.022.
[62] Q. Wu, M. Maskus, F. Pariente, F. Tobalina, V.M. Fernández, E. Lorenzo, H. D. Abruña, Electrocatalytic oxidation of NADH at glassy carbon electrodes modified with transition metal complexes containing 1,10-Phenanthroline-5,6-dione ligands, Anal. Chem. (Washington) 68 (20) (1996) 3688–3696, https://doi.org/10.1021/ac960395y.
[63] J.A. Steele, R.A. Lewis, In situ micro-Raman studies of laser-induced bismuth oxidation reveals metastability of beta-Bi2O3 microislands, Opt. Mater. Express. 4 (2014) 2133, https://doi.org/10.1364/OME.4.002133.
[64] C. Gibaja, D. Rodriguez-San-Miguel, P. Ares, J. Gómez-Herrero, M. Varela, R. Gillen, J. Maultzsch, F. Hauke, A. Hirsch, G. Abellán, F. Zamora, Few-layer Antimonene by liquid-phase exfoliation, Angew. Chem. Int. Ed. 55 (2016) 14345–14349, https://doi.org/10.1002/anie.201605298.
[65] I. Torres, M. Alcaraz, R. Sanchis-Gual, J.A. Carrasco, M. Fickert, M. Assebban, C. Gibaja, C. Dolle, D.A. Aldave, C. Gómez-Navarro, E. Salagre, E. García Michel, M. Varela, J. Gómez-Herrero, G. Abellán, F. Zamora, Continuous-flow synthesis of high-quality few-layer Antimonene hexagons, Adv.Funct.Mater. 31 (2021) 2101616, https://doi.org/10.1002/adfm.202101616.
[66] A.C. Ferrari, J.C. Meyer, V. Scardaci, C. Casiraghi, M. Lazzeri, F. Mauri, S. Piscanec, D. Jiang, K.S. Novoselov, S. Roth, A.K. Geim, Raman Spectrum of graphene and graphene layers, Phys. Rev. Lett. 97 (2006) 187401, https://doi.org/10.1103/PhysRevLett.97.187401.
[67] N. Kuhar, S. Sil, S. Umapathy, Potential of Raman spectroscopic techniques to study proteins, Spectrochim. Acta A Mol. Biomol. Spectrosc. 258 (2021) 119712, https://doi.org/10.1016/j.saa.2021.119712.
[68] Y. Wang, M. Shi, D. Bao, F. Meng, Q. Zhang, Y. Zhou, K. Liu, Y. Zhang, J. Wang, Z. Chen, D. Liu, Z. Jiang, M. Luo, L. Gu, Q. Zhang, X. Cao, Y. Yao, M. Shao, Y. Zhang, X. Zhang, J.G. Chen, J. Yan, Q. Jiang, Generating defect-rich bismuth for enhancing the rate of nitrogen electroreduction to Ammonia, Angew. Chem. Int. Ed. 58 (2019) 9464–9469, https://doi.org/10.1002/anie.201903969.
[69] R.W. Joyner, M.W. Roberts, S. Singh-Boparai, X-ray induced effects during the oxidation of Bi(0001), Surf. Sci. 104 (1981) L199–L203, https://doi.org/10.1016/0039-6028(81)90118-7.
[70] P.E. Peterson, J. Pierce, T.J. Smith, Crystallization and characterization of bovine liver glutamate dehydrogenase, J. Struct. Biol. 120 (1997) 73–77, https://doi.org/10.1006/jsbi.1997.3899.
[71] L. Blasi, L. Longo, P.P. Pompa, L. Manna, G. Ciccarella, G. Vasapollo, R. Cingolani, R. Rinaldi, A. Rizzello, R. Acierno, C. Storelli, M. Maffia, Formation and characterization of glutamate dehydrogenase monolayers on silicon supports, Biosens. Bioelectron. 21 (2005) 30–40, https://doi.org/10.1016/j.bios.2004.10.012.
[72] L. Meng, P. Wu, G. Chen, C. Cai, Y. Sun, Z. Yuan, Low potential detection of glutamate based on the electrocatalytic oxidation of NADH at thionine/single-walled carbon nanotubes composite modified electrode, Biosens. Bioelectron. 24 (2009) 1751–1756, https://doi.org/10.1016/j.bios.2008.09.001.
[73] S. Chakraborty, C. Retna Raj, Amperometric biosensing of glutamate using carbon nanotube based electrode, Electrochem.Commun. 9 (2007) 1323–1330, https://doi.org/10.1016/j.elecom.2007.01.039.
[74] K. Sato, T. Kamijo, S. Takahashi, T. Sato, Comparison of NAD with NADP-dependent glutamate dehydrogenase, and CNT with rGO-modified electrodes, for the construction of glutamate sensors, Electroanalysis 30 (2018) 2237–2240, https://doi.org/10.1002/elan.201800160.S.